ON THE ENHANCEMENT OF THE IMPACT TOUGHNESS OF A319 ALLOYS: ROLE OF Mg CONTENT AND MELT TREATMENT

F. J. Tavitas-Medrano and F. H. Samuel
Université du Québec à Chicoutimi, Chicoutimi, QC, Canada

H. Doty
General Motors Materials Engineering, Pontiac, MI, USA

S. Valtierra
Nemak, S.A., P.O. Box 100, 66221 Garza Garcia, NL, Mexico

DOI 10.1007/s40962-016-0098-3

Abstract

The present work was performed on low Fe-low Mg A319 alloys. The results show that the A319-type aluminum alloy with the optimum combination of impact properties consists of a Sr-modified alloy with additions of Mg. The Sr-modification process does not affect the aging behavior of the alloy, while the addition of Mg enhances its response to artificial aging. The strengthening effect observed in the alloy is due mainly to the presence of θ-Al_2Cu particles which precipitate in the form of needles and plates. The degree of strengthening that may be obtained depends directly on the amount and homogeneity of the θ-Al_2Cu phase. The alloy does not exhibit the common peak-over-aging conditions normally found in the literature. This is due to the presence of sequential precipitation of different species during the aging process, whereas hardness is less sensitive to melt treatment conditions, and aging treatment has a significant influence on the alloy hardness. In the non-modified alloy, the Si particles may be cleaved during impact testing resulting in poor toughness. Modification with Sr improves the alloy resistance to fracture during impact testing due to the larger volume fraction of the ductile aluminum matrix compared to non-modified alloys.

Keywords: *hardness, impact toughness, aluminum alloys, melt treatment, precipitation hardening*

Introduction

An extensive study was carried out by Li et al.[1,2] on the mechanical properties of A319-type alloys. Their findings showed that factors such as a decrease in cooling rate and the addition of Sr are beneficial, while the presence of Fe-containing phases such as β-Al_5FeSi and the segregation of the $CuAl_2$ phase, as well as its incomplete dissolution, are detrimental to the tensile properties. In regard to impact properties, Sr modification is beneficial, while the β-Al_5FeSi phase may act as a crack initiation site, thereby reducing the impact toughness of the material. The elongation in tensile tests may be related to the impact toughness of the material: the more ductile the material, the higher the impact toughness values will be. The study also included a comparison of two heat treatment conditions, T5 and T6; the main difference being the presence of the solution heat-treating stage and water quenching in the T6 condition. The results showed that all of the properties analyzed are significantly improved when treated using the three stages of a typical T6 heat treatment regime.

Several studies[3–9] have been carried out to analyze the effects of experimental aging cycles on aluminum alloys. These studies claim that certain mechanical properties such as tensile strength, hardness and impact toughness may display improvements of up to 30 % as compared to conventional aging cycles. The non-conventional cycles consist in pre-aging the alloy (namely, aging before the peak aging condition is reached); then maintaining it at a low temperature, anywhere between room temperature and 65 °C, for extended periods of time, from a few hours to a few weeks, and finally resuming the aging to either the peak or overaging condition. These experimental aging

cycles have a beneficial effect on some of the alloys studied. More details, however, are not provided for specific alloy systems; also, these investigations mainly cover wrought alloys, and only a few cast alloys.

The effect of Mg additions on the aging behavior of A319-type alloys was studied by Ouellet and Samuel.[10] They determined that addition of 0.45 % Mg enhances the alloy response to heat treatment, particularly in the T6 condition where improvements of more than 40 % in strength are obtained in samples that contain Mg, in comparison with samples treated at the same temperature and time (8 h at 180 °C) containing very low levels of Mg, about 0.06 %.

Considering that alloy A319 is commercially important and given its complexity, resulting from the presence of silicon, copper, magnesium and strontium, the study of its precipitation behavior, as well as of the mechanisms which operate during aging, will provide a more in-depth and detailed understanding of the response of the alloy in the context of mechanical properties.[11–14]

The main objective of this study is to examine the effect of increasing the Mg content, as well as varying the melt treatment parameters mainly degassing process, Sr modification, grain refining, and hydrogen content on the impact toughness of A319 alloy. In certain cases, it was deemed important to correlate the total absorbed energy with either the alloy ductility or hardness.

Experimental Procedure

The chemical composition of the as-received A319 alloy is shown in Table 1. The alloy was received in the form of 12.5 kg ingots, which were melted using an electrical resistance furnace. The melting temperature was maintained at 730 ± 5 °C (to insure high fluidity of the liquid metal and hence sounder castings). The molten metal was degassed using pure dry argon injected into the molten metal (0.85 m^3/h) by means of a rotary graphite impeller. The degassing time/speed was kept constant at 30 min/150 rpm in order to obtain a lower hydrogen level of ~0.1 mL/100 g in the melt.

Measured amounts of Mg in the form of pure metal, Al-10 %Sr and Al-5wt%Ti-1wt%B master alloys (in the form of cut rods) were added to the molten metal after degassing. Samples for chemical analysis were also extracted simultaneously for each melt/casting produced. The chemical compositions representing the average of three spectrometric analyses (using Spectrolab Jr CCD Spark Analyzer) for each of the alloys investigated are listed in Table 2. The melt hydrogen level was increased through the addition of raw potatoes to the melt to obtain levels of 0.2 mL/100 g (low) and 0.4 mL/100 g (high) and determined using the Leco sub-fusion technique.

Table 1. Chemical Composition of A319 Alloy

Element (wt%)							
Si	Cu	Fe	Mn	Mg	Zn	Ti	Sr
6.15	3.53	0.09	0.001	0.05	0.008	0.07	0.0001

For alloys ADM and ADMS, a permanent mold of the type ASTM B-108 was used to cast 250 tensile test bars. The samples were solution heat treated at 495 °C for 8 h in a forced-air Blue M electric resistance furnace where the temperature could be controlled to within ±1 °C, and then were immediately quenched in warm water at 60 °C; after that, the artificial aging treatment was carried out. After cooling the samples from the solution heat treatment stage, they were stored in a freezer at approximately −20 °C until the artificial aging cycle was carried out, in order to avoid natural aging effects. The results obtained from the conventional artificial aging treatments used served as a baseline for comparison with the new proposed cycles. These cycles were applied at five different temperatures (150, 170, 190, 220 and 240 °C) for 2, 4, 6 and 8 h.

Five tensile test bars were used for each alloy/heat treatment condition. These bars were pulled to fracture at room temperature using an MTS™ Servohydraulic mechanical testing machine at a strain rate of 4×10^{-4}/s. A strain gauge extensometer was attached to the test bars to measure alloy ductility. The yield strength (measured at 0.2 % offset strain), the ultimate tensile strength and the total percent of elongation before fracture were obtained by means of a data acquisition system attached to the machine.

A star-like metallic mold which provided a high solidification rate was used to prepare the impact and the hardness test specimens. Metallographic samples were prepared for the alloys studied. Each casting provides ten impact bars which are cut from the casting and then machined to the required ASTM E23 specifications to conduct Charpy impact tests subsequently. Hardness test specimens measuring 10 mm × 10 mm × 55 mm were cut from the casting and polished with fine sandpaper to remove any machining marks.

The hardness and impact test samples prepared for each alloy composition were solution heat treated at 495 °C for 8 h, followed by quenching in warm water at 65 °C, and artificial aging for 5 h at 155, 180, 200, 220 and 240 °C. All heat treatments were conducted in a forced-air Blue M electric furnace equipped with a programmable temperature controller, accurate to ±2 °C. For each individual heat treatment condition, five test bars were used.

The hardness measurements were taken on the as-cast and heat-treated samples using a Brinell hardness tester,

Table 2. Chemical Composition of the Alloys Used in The Present Study

Sample code	Elements (wt%)									
	Si	Fe	Cu	Mn	Mg	Cr	Ti	B	Sr	Al
A &AD	5.59	0.17	3.11	<0.0005	0.071	<0.0005	0.07	0.0004	**0.0005**	91.0
ADM	5.57	0.18	3.4	<0.0005	**0.45**	<0.0005	0.15	0.0400	0.0005	91.0
ADMS	5.57	0.19	3.2	<0.0005	**0.43**	<0.0005	**0.15**	0.0400	**0.0200**	90.5
ADT1	5.57	0.18	3.13	<0.0005	0.043	<0.0005	**0.13**	**0.0400**	0.0002	90.9
ADS	5.55	0.18	3.05	<0.0005	0.045	<0.0005	0.10	<0.0002	**0.0161**	91
ADTS	5.79	0.19	3.22	<0.0005	0.038	<0.0005	**0.15**	**0.040**	**0.0186**	90.6
ADT2	5.39	0.20	3.06	<0.0005	0.040	<0.0005	**0.23**	**0.0360**	<0.0000	91.1
ADT2S	5.68	0.21	3.16	<0.0005	0.043	<0.0005	**0.25**	**0.0338**	0.0134	90.7
ADH†	5.80	0.18	3.07	0.0071	0.039	<0.0005	0.07	<0.0002	0.0002	90.8
ADH4††	5.62	0.18	3.02	0.0053	0.042	<0.0005	0.07	<0.0002	<0.0000	91.2

Bold numbers indicate specific additions made to the base alloy

† Alloy AD containing low hydrogen level (0.2 ml/100g Al)

†† Alloy AD containing high hydrogen level (0.4 ml/100g Al)

applying a steel ball of 10 mm diameter and a load of 500 kgf for 30 s. An average of four readings obtained from two perpendicular surfaces was taken to represent the hardness value in each case.

A computer-aided instrumented SATEC SI-1 Universal Impact Testing Machine (SATEC Systems Inc., Model SI-1D3) was used to carry out the impact tests. A data acquisition system connected to the impact machine monitored the dynamic behavior of the test specimen and measured the load and energy values as a function of time. Samples for metallographic observations were sectioned from the impact-tested bars of all the alloys studied, about ~10 mm below the fracture surface. The samples were mounted in bakelite and polished to a fine finish.

The microstructures of the polished sample surfaces were examined using an optical microscope linked to a Clemex image analysis system. The eutectic silicon particle characteristics, including area, length, aspect ratio, roundness, and density, were measured and quantified. For each sample, 50 fields at a magnification of 500× were examined, so as to cover the entire sample surface in a regular and systematic manner. In addition, porosity measurements were taken, over 50 fields per sample, at a magnification of 100×. The porosity parameters measured were percentage porosity, pore area, and pore length. As a rule, the outer edges of the sample were avoided in taking these measurements so as to eliminate any distortions which might occur in the peripheral regions. Some selected samples were examined using a Hitachi SU-8000 field emission gun scanning electron microscope (FESEM). Prior to examination, these samples were re-polished using ion bombardment to remove surface oxides.

For measurements of grain size, the polished samples were chemically etched using Keller's reagent (66 vol% HNO_3, 33 vol% HCl, and 1 vol% HF), diluted with water to slow down the etching process. Once etching was completed, the sample surfaces were rinsed, dried and then photographed using a set-up consisting of four projectors emitting red, blue, green and yellow light. The grain sizes were measured from the digital photographs using Sigma Scan Pro 4.0 software, employing a method similar to the line intercept method. The grain size for each sample was obtained as the average of 80 readings. Selected samples were examined using transmission electron microscopy to identify the precipitates on a very small scale, employing a JEOL™ JEM-2100F electron microscope equipped with an advanced control system which permits the integration of an EDAX™ chemical analysis system, scanning transmission electron microscope (STEM), and electron energy loss spectroscopy (EELS). The microscope was operated at an acceleration voltage of 200 keV.

Results and Discussion

Effect of Mg Addition

Figure 1 shows the variation in elongation and total absorbed impact energy values for grain refined A319 base alloy (coded ADT alloy), obtained after continuous aging over the same range of aging temperatures (150–240 °C) and times. The primary Y-axis represents percentage elongation, and the secondary Y-axis represents the total absorbed impact energy in joules. As can be seen, the elongation and impact toughness values also improve on going from the as-cast state to the solution heat-treated

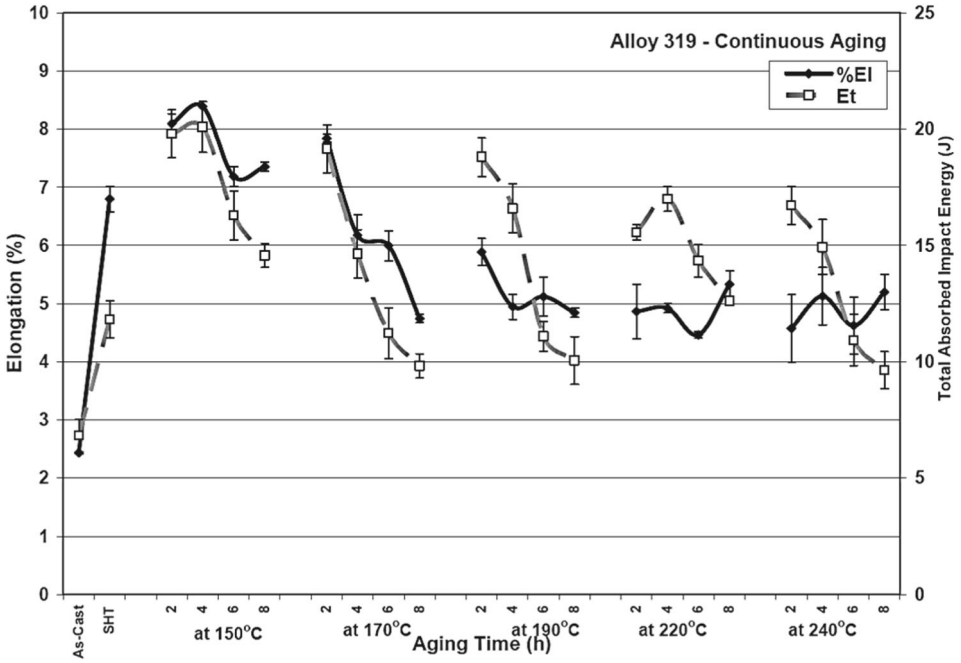

Figure 1. Average values of percentage elongation (%El) and total absorbed impact energy (E_t) obtained for the ADT base alloy under different heat treatment conditions (using continuous aging cycles).

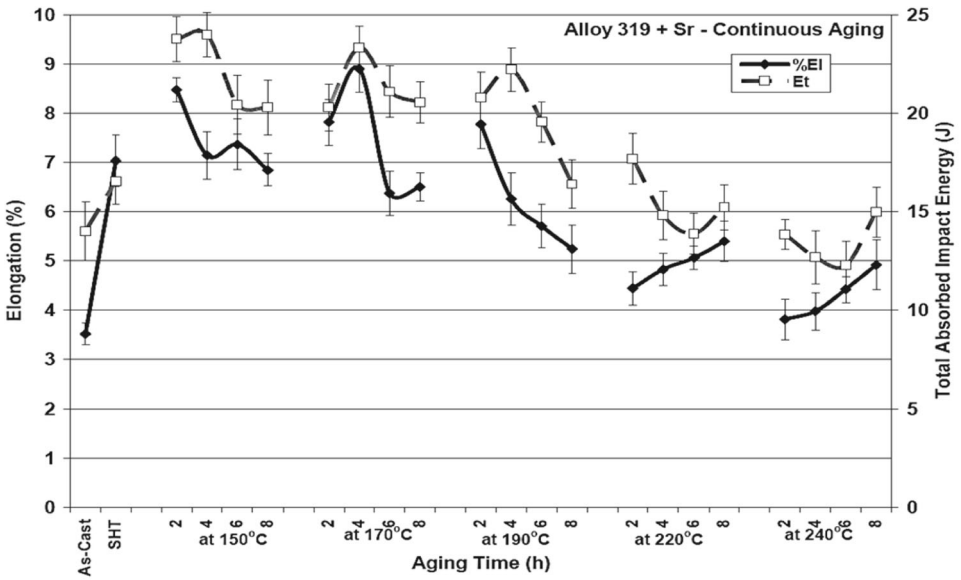

Figure 2. Average values of percentage elongation (%El), and total absorbed impact energy (E_t) obtained for the ADTS alloy under different heat treatment conditions (using continuous aging cycles).

(T4) condition. Peak values for both properties are attained when artificial aging is carried out at 150 °C for 4 h, after which the values tend to decrease over time. The improvement in the impact toughness values and in the elongation values may be explained by the even distribution of microconstituents and their dissolution in the aluminum matrix achieved through the solution heat treatment/quenching step.[1,2] Also, the fragmentation, dissolution and spheroidization processes taking place during solution heat treatment reduce the amount of acicular particles such as eutectic Si and Fe-containing phases initially existing in the as-cast sample, as well as the amount of undissolved Cu-containing phases. These phases are hard particles that play a key role in the fracture propagation process and may act as crack initiation sites.[2,15–18]

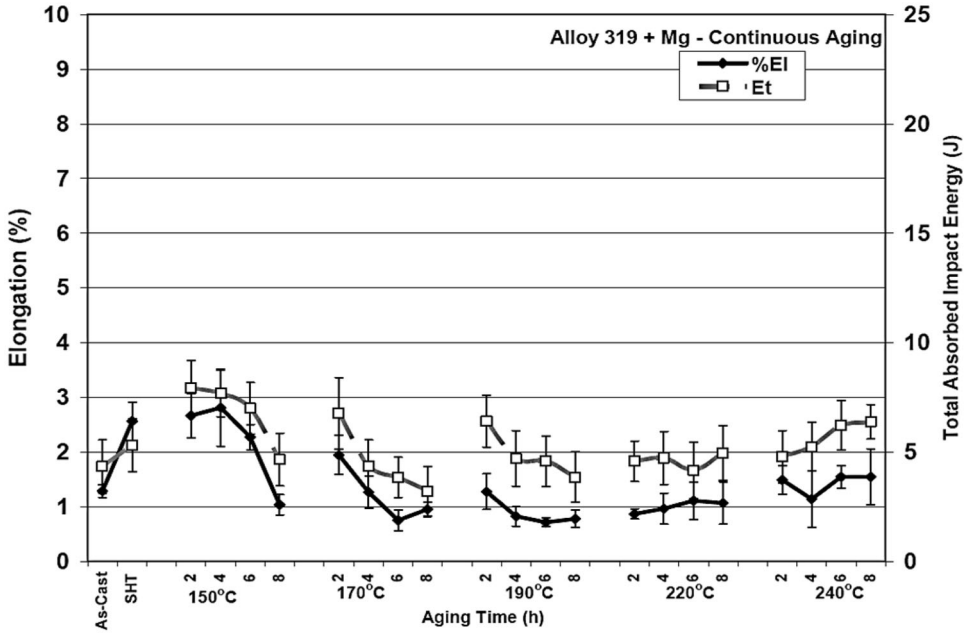

Figure 3. Average values of percentage elongation (%El), and total absorbed impact energy (E_t) obtained for the ADM alloy under different heat treatment conditions (using continuous aging cycles).

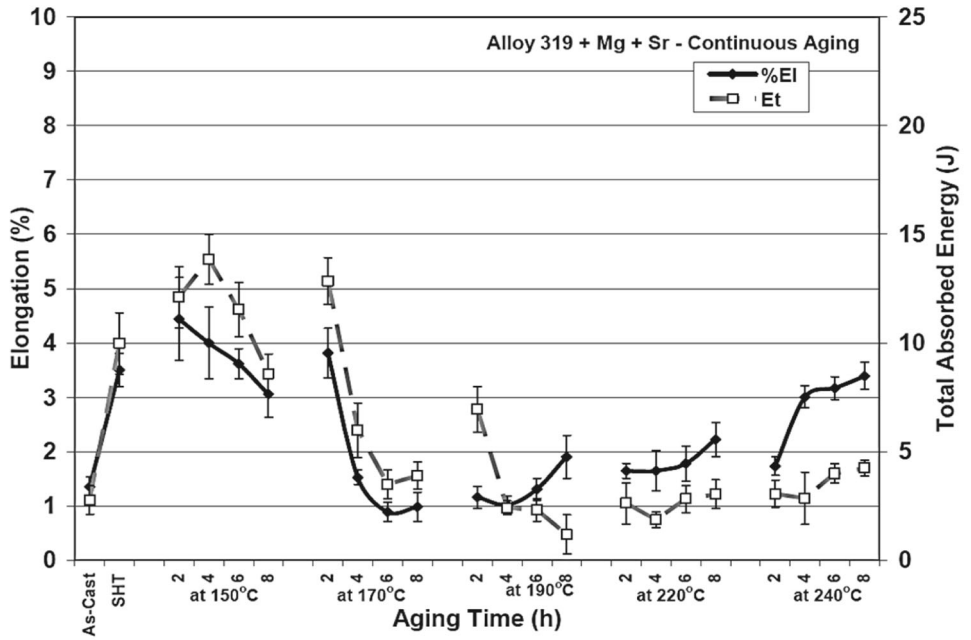

Figure 4. Average values of percentage elongation (%El), and total absorbed impact energy (E_t) obtained for the ADMS alloy under different heat treatment conditions (using continuous aging cycles).

Figure 1 also shows that when artificial aging is carried out at 170 °C, both properties decrease with increasing aging time. The same behavior may be observed for the aging cycles at 190 °C, but the decrease is more marked for the impact toughness. Such a decrease is expected since it is in these aging cycles that the highest strength values are obtained. At higher artificial aging temperatures, i.e., 220 and 240 °C, impact toughness values again decrease with time. Elongation, however, shows a slight recovery at long aging times, i.e., 8 h at 220 °C.

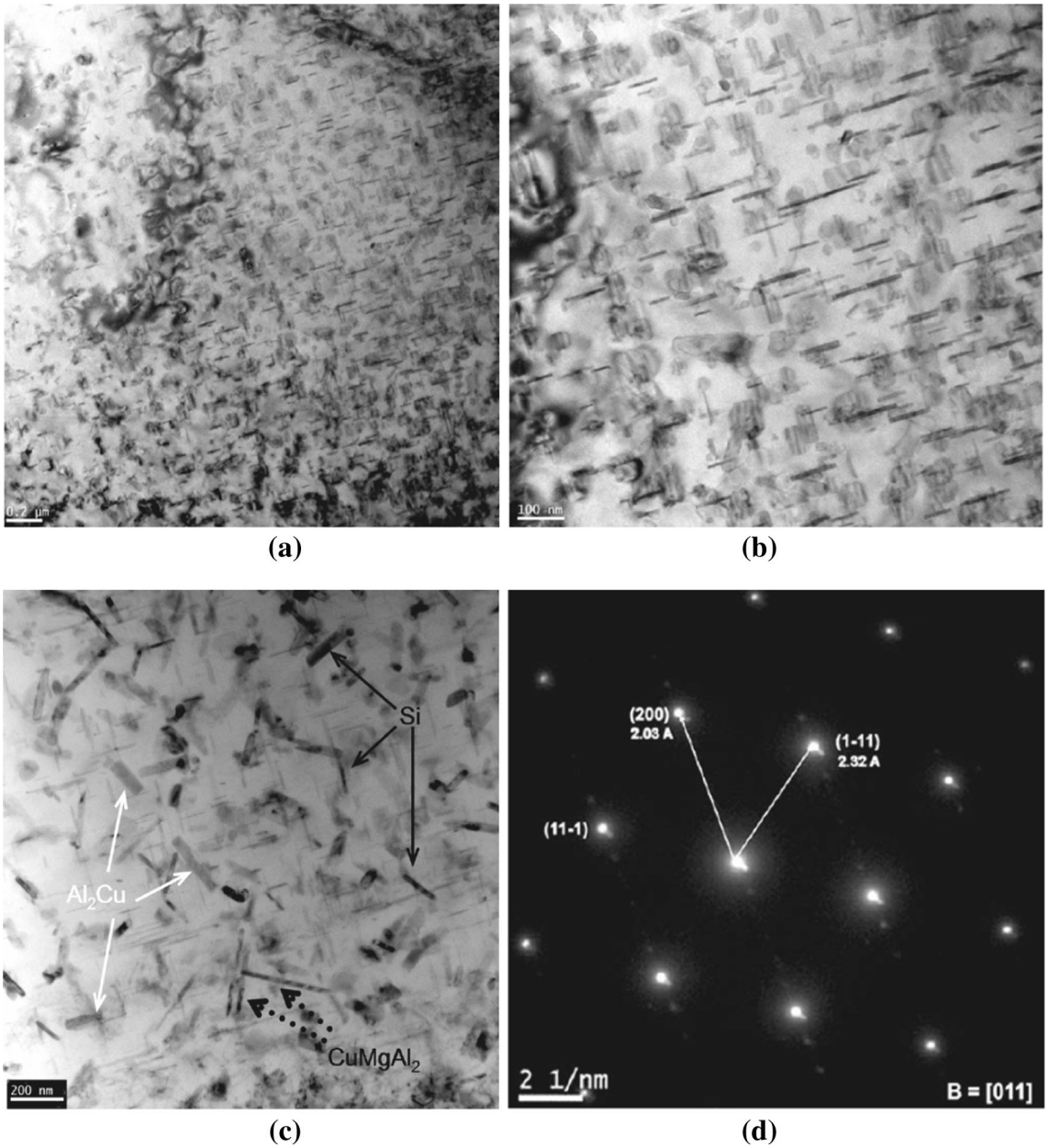

Figure 5. (a) Bright field TEM image of the microstructure observed in the sample aged at 240 °C for 8 h (alloy ADMS), (b) Bright field TEM image at an increased magnification of (a), (c) Precipitation of Si, Al_2Cu and $CuMgAl_2$ phases, (d) selected area diffraction pattern of (a) showing additional spots belonging to the θ-Al_2Cu phase.

Table 3. Average Grain Size as a Function of the Added Grain Refiner

Sample code	Grain size (μm)	Standard deviation (μm)
AD	678	39
ADT1	544	30
ADT2	214	24

Figure 2 shows the variation in elongation and total absorbed impact energy values for the grain refined, Sr-modified A319 alloy (coded ADTS alloy) when subjected to continuous aging cycles over the same range of aging temperatures and times. It will be observed that the values are higher in this case compared to those exhibited by the base alloy. This is to be expected, since these properties depend to a high degree on the morphology and distribution of the brittle Si, Fe and Cu phases mentioned previously, which are responsible for the fracture in this type of alloy.[2,19] Thus, modifying the eutectic silicon phase is expected to improve the ductility and impact toughness of the alloy as evidenced by Figure 2.

From the initial improvement in elongation and absorbed energy values after solution heat treatment, a peak may be

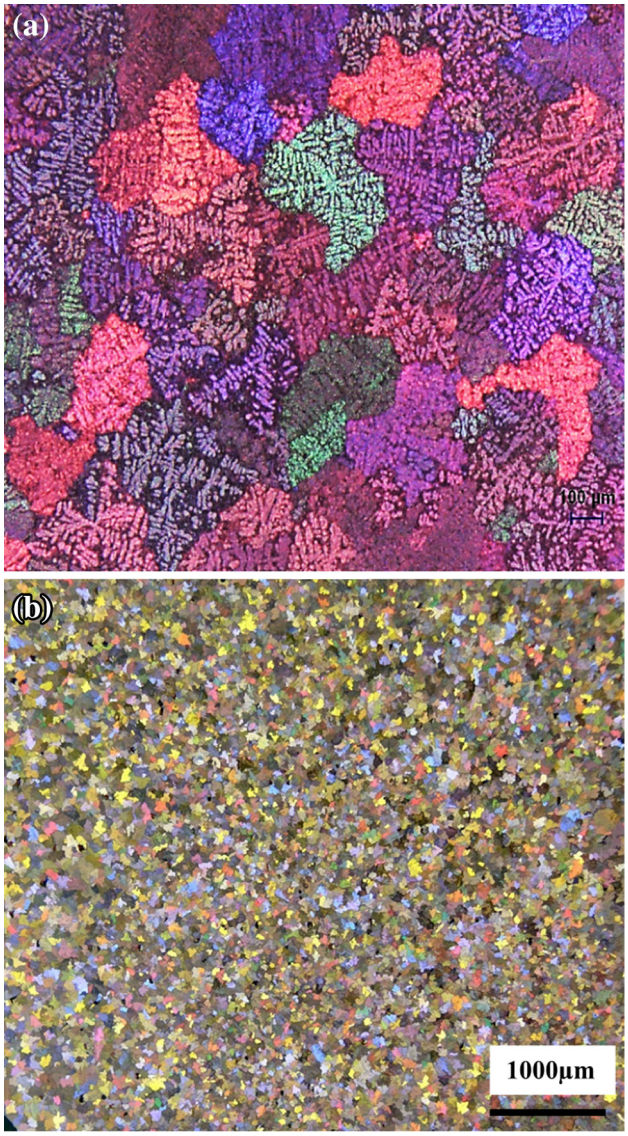

Figure 6. Macrostructure of the grains obtained from (a) 0.02 % Ti (AD), (b) 0.25 %Ti (ADT2) additions.

seen after aging at 150 °C for 2 h. It is for this aging cycle that the highest impact toughness is observed. Increasing the aging time at the same temperature is seen to decrease the value obtained. Aging at 170 °C shows an improvement in toughness for the first 4 h, where the peak is observed, thereafter the values decrease over time. The same behavior, i.e., decrease in elongation and impact energy over time, is observed when aging is carried out at 190 °C. At higher aging temperatures, i.e., 220 and 240 °C, a slow recovery in elongation and toughness is observed when aging is carried out for long periods, such as 6 and 8 h.

The corresponding values of elongation and total absorbed impact energy for the best T6 treatment, 4 h at 150 °C, are 7.13 % and 24 J, respectively. Those for the best T7 heat treatment, 2 h at 240 °C, are 3.81 % and 13.83 J, respectively.

Figure 3 shows the variation in percentage elongation and total absorbed impact energy values obtained for the A319 + Mg alloy (coded ADM alloy) after continuous aging over the range of temperatures studied. From a comparison of Figure 3 with Figures 1 and 2, it is evident that these values tend to be lower than those exhibited by the base A319 and Sr-modified alloys.[20,21] While the addition of Mg increases the strength and hardness of the alloy, it does so at the expense of ductility.[10,22–24]

Starting from the as-cast condition, an improvement in properties is obtained with the T4 treatment (solution heat treatment). Additional aging at 150 °C improves the values still further up to an aging time of 4 h; beyond this point, the values begin to decrease. The same tendency is observed when aging at 170 °C, over the same range of times. At 190 °C aging temperature and after 2 h of aging, the elongation achieved is the same as that observed in the as-cast condition. Increasing the aging time to 4 h slightly reduces the elongation which thereafter remains more or less stable for longer aging times. A similar behavior may also be observed at 220 °C, since the values remain unchanged over the aging time. Finally, at 240 °C, a slight recovery can be observed for both the percent elongation and the absorbed impact energy. The corresponding values of elongation and total absorbed impact energy for the best T6 treatment, i.e., 8 h at 170 °C, are 0.95 % and 3.21 J, respectively. The corresponding values for the best T7 treatment, i.e., 2 h at 240 °C, are 1.49 % and 4.79 J.

Figure 4 shows the variation in elongation and total absorbed impact energy values for the Sr-modified A319 + Mg alloy (coded ADMS alloy) obtained after continuous aging over the range of temperatures and times studied. In comparison with the unmodified A319 + Mg alloy, the modified alloy (A319 + Mg + Sr) shows higher ductility and absorbed impact energy values, as expected.[25]

Due to the presence of Mg, both alloys exhibit the same response to aging: an increase in properties is initially observed on going from the as-cast to the solution heat-treated condition. Aging at 150 °C and 170 °C, however, shows a loss in properties over the aging times studied. The highest strength and microhardness values are observed after aging at 170 °C for 8 h, which represents the best T6 treatment in this case. The elongation and impact absorbed energy values are 0.98 % and 3.21 J, respectively.

Aging at 190 °C produces an increase in elongation values when aging is carried out for longer times, i.e., 6 h and 8 h, whereas the absorbed impact energy values continue to decrease over time to reach a minimum after 8 h of aging at this same temperature. At higher aging temperatures, i.e., 220 °C and 240 °C, the properties improve with increasing aging time. The T7 condition for this alloy, i.e.,

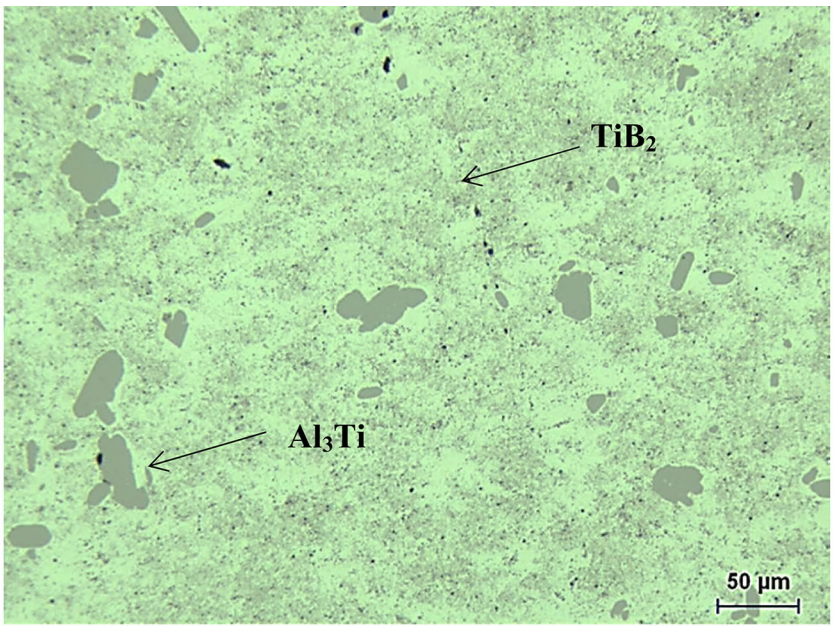

(a)

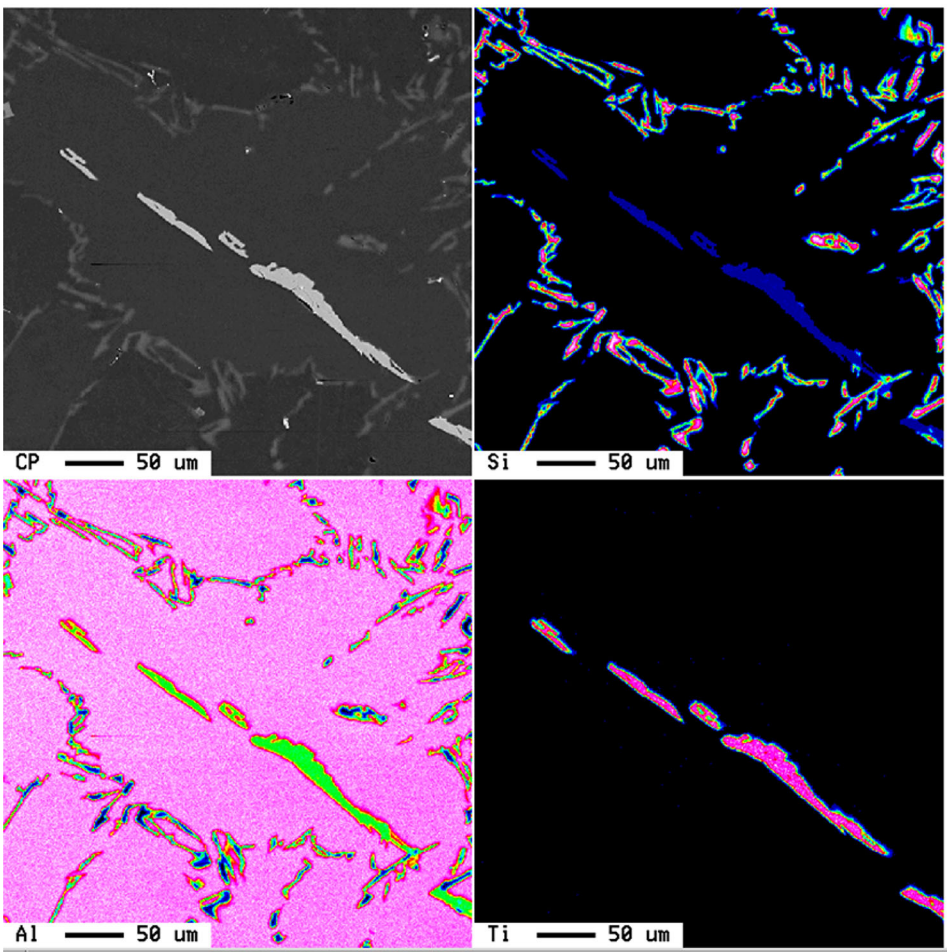

(b)

Figure 7. (a) Microstructure of the Al-Ti-B master alloy for the addition of titanium as a grain refiner in this work, and (b) backscattered electron image (top left) and distribution of Al, Ti and Si in a Ti–rich phase platelet in the ADT2 alloy sample.

Table 4. Characteristics of Eutectic Si Particles

Sample code	Particle area (μm^2)		Particle length (μm)		Roundness (%)		Aspect ratio		Density (particles/mm^2)
	Average	SD*	Average	SD	Average	SD	Average	SD	
(a) In the as-cast condition									
A	18.19	48.99	6.89	13.26	67.10	32.36	2.55	1.52	2365
AD	22.73	44.01	10.00	14.25	56.78	33.41	2.71	1.60	3414
ADT1	17.16	48.08	6.59	13.17	67.38	30.89	2.41	1.26	3738
ADS	3.61	8.48	2.79	2.91	74.67	23.75	1.91	0.73	15212
ADTS	7.14	14.41	4.44	4.50	58.89	28.85	2.27	1.12	8285
ADH	25.65	56.15	9.64	16.08	60.93	33.06	2.62	1.52	2764
ADH4	22.34	53.65	8.28	15.20	66.51	33.31	2.36	1.34	3177
ADT2	17.01	38.01	7.56	12.88	63.62	32.70	2.55	1.55	3937
ADT2S	3.77	8.60	3.08	3.46	71.09	25.24	2.07	0.89	21239
(b) After solution heat treatment									
A	33.34	63.25	10.39	15.92	67.40	31.64	2.30	1.41	2146
AD	33.69	49.27	12.57	13.83	55.40	30.77	2.85	1.68	2668
ADT1	48.22	81.03	14.39	19.63	60.25	32.42	2.49	1.52	1771
ADS	6.71	12.75	3.54	3.31	81.25	18.81	1.71	0.66	10679
ADTS	11.71	18.46	5.04	4.58	70.97	24.76	1.89	0.83	6492
ADH	39.42	77.80	12.53	20.49	64.80	31.89	2.41	1.50	1969
ADH4	39.05	59.32	13.14	16.34	59.76	32.54	2.70	1.64	2139
ADT2	29.75	43.23	11.82	13.74	56.29	31.61	2.74	1.60	2532
ADT2S	6.53	11.70	3.52	3.38	81.27	18.55	1.68	0.63	13512

* Standard deviation

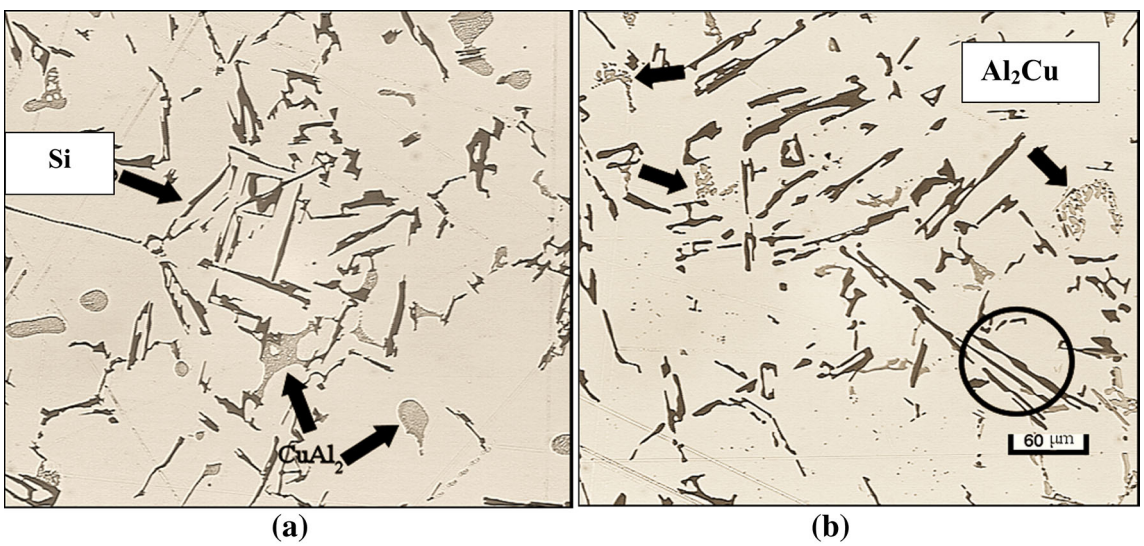

Figure 8. Optical microstructures of the AD alloy (a) in the as-cast condition, (b) after solutionizing treatment. Black circled area shows fragmentation of the non-modified Si particles.

2 h at 240 °C, yields an elongation of 1.73 % and 3.06 J for the total absorbed impact energy.

Figure 5 presents the image of the Al_2Cu precipitates in the form of needles present in the ADMS alloy sample aged at 240 °C for 8 h. The Al_2Cu needles observed have an average size of 35 × 5 nm. They precipitate in the ⟨100⟩ directions of the matrix,[23,26] and although it may appear that there is a second kind of particle precipitating at about 90° to the needles, it is the same phase but seen from a

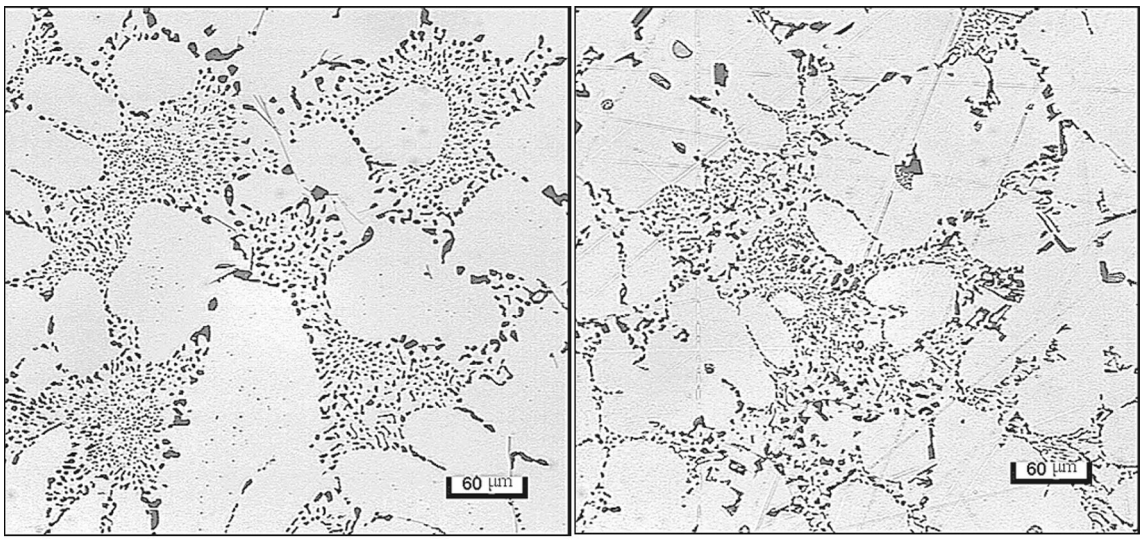

Figure 9. Optical microstructures of ADTS alloy (a) in the as-cast condition, (b) after solutionizing treatment.

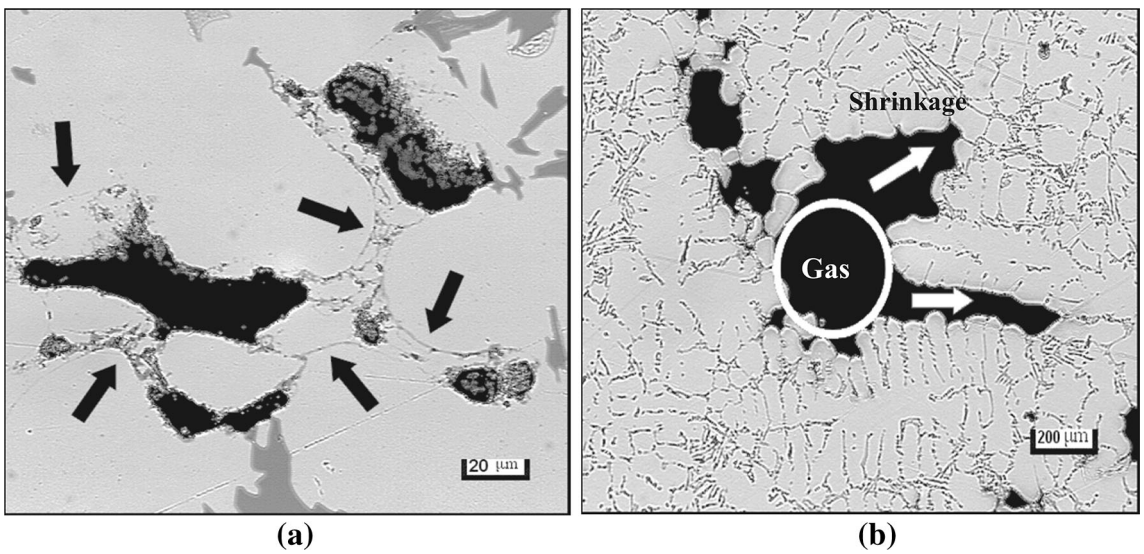

Figure 10. Optical microstructures showing: (a) the presence of large oxide films (arrowed) associated with porosity in the base alloy A, (b) the development of a gas pore into shrinkage cavities during solidification of high-hydrogen containing ADH4 alloy.

perpendicular direction; these particles appear to have a plate-like morphology because of the two-dimensional projection due to the fact that these images were not taken near the [001] zone axis but near a [011] axis-Figure 5d.

Effect of Melt Treatment

Table 3 shows the response of the base alloy (coded AD) to the added amounts of grain refiners. According to Wu et al.[27] and Sigworth and Guzowski,[28] the addition of grain refiner in the form of Al-5 %Ti-1 %B leads to continuous decrease in the alloy grain size till it reaches a certain concentration beyond which further addition has no effect on the grain size. In the present study, three concentrations were selected, viz. 0.007 % Ti, 0.15 %Ti and 0.25 %Ti. Figure 6 reveals significant reduction in the alloy grain size (about 80 %) when the grain refiner (measured by the added amount of Ti % was increased from 0.07 % to 0.25 %Ti. In certain cases, the Al_3Ti part of the Al–Ti-B master alloy would react with the eutectic Si leading to the formation of $Ti(Al,Si)_3$ phase (containing about 64.7 at % Al, 24.26 at %Ti, 10 at %Si), as shown in Figure 7. The

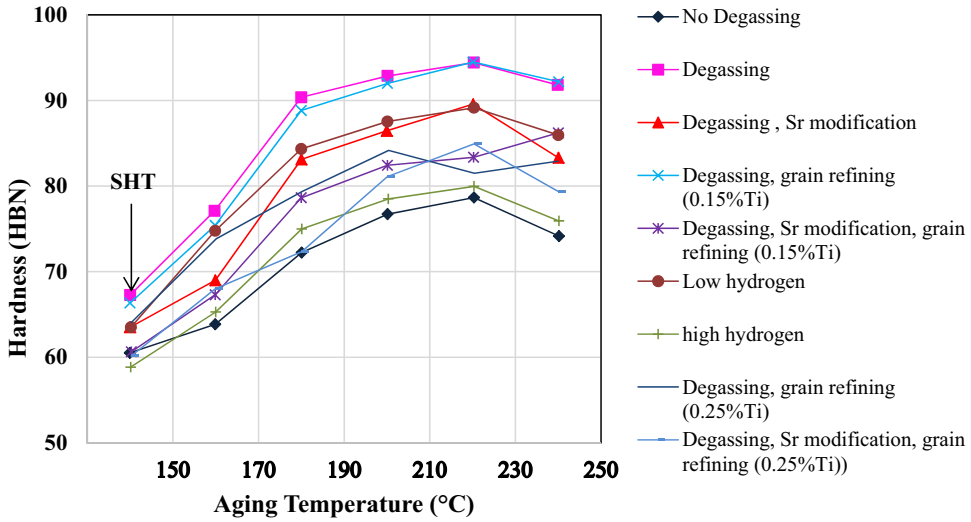

Figure 11. Variation in the alloy hardness as a function of the applied melt treatment and aging temperature-aging time 5 h.

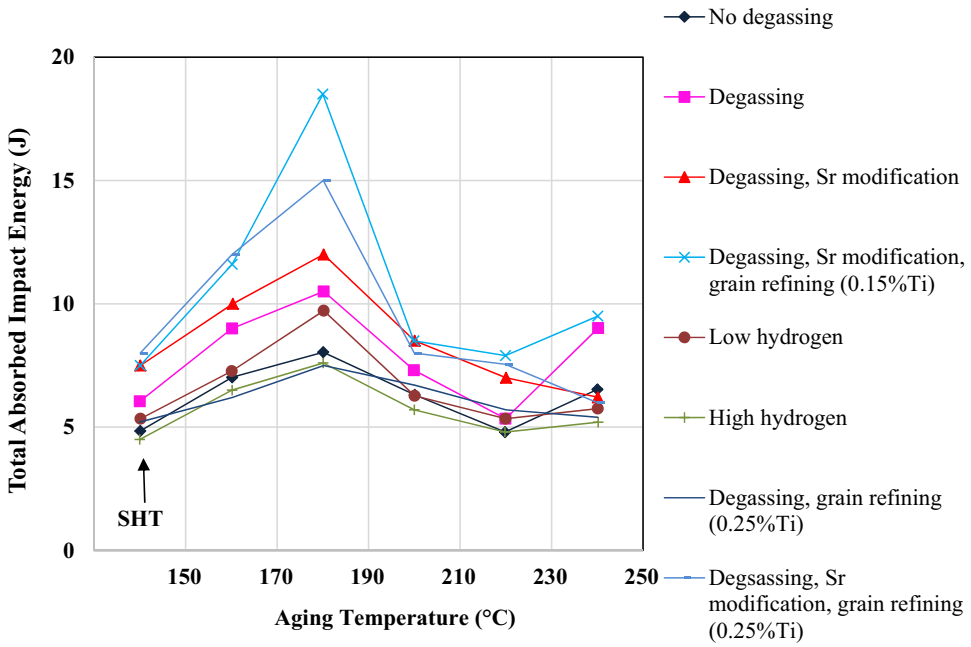

Figure 12. Variation in the alloy total absorbed energy (E_t) as a function of the applied melt treatment and aging temperature-aging time 5 h.

occurrence of this reaction would reduce the effectiveness of Ti-containing grain refining master alloys.

Table 4a lists the variation in the characteristics of the eutectic Si particles as a function of the applied melt treatment in the as-cast condition, whereas Table 4b exhibits the variation is the same parameters after solution heat treatment. Based on these tables, it is evident that Sr addition is the more effective agent in modifying the size and morphology of the eutectic Si particles. Solution heat treatment would result in coarsening the particles regardless the modification condition. The fact that this alloy was solutionized at a relatively low temperature, i.e., 495 °C may slow down the spheriodization process reported for 356 alloys.[29] Figures 8 and 9 clearly confirm these observations; note the dissolution of the Al_2Cu phase in Figure 9. Figure 10 illustrates the importance of proper degassing in order to remove the oxide films and hydrogen to obtain sound castings with minimum porosity.

Figure 11 demonstrates the effect of the applied melt treatments on the alloy hardness (as a strength parameter). It may be seen that the as-received alloy A revealed the lowest hardness regardless the aging temperature. This may be attributed to the presence of heavy oxide films in the alloy (as displayed in Figure 10). The best result is

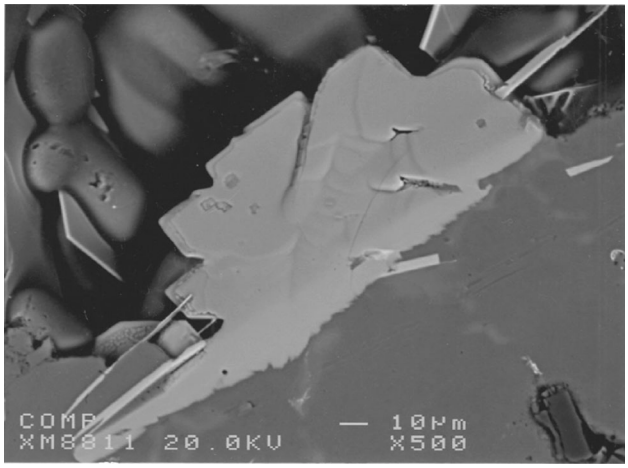

Figure 13. Backscattered image of ADT2 alloy (containing 0.25 %Ti) revealing the plate-like shape of Al_3Ti phase.

obtained when the alloy is degassed and grain refined. Modification with Sr (Figure 11) seems to have relatively less effect on the alloy hardness compared to grain refining.

Figure 12 illustrates the variation in the total energy of the alloys studied, following aging at different temperatures. Three main observations can be made:

1. Unlike in the case of hardness, the addition of Sr resulted in a significant improvement in the degassed alloys due to changes in the morphology of the eutectic Si particles from acicular (AD alloy, degassing, Figure 8a) to fibrous form (ADS alloy, degassing and Sr modification).
2. Increasing the amount of added grain refiner (0.25 %Ti) leads to precipitation of large platelets of Al_3Ti phase (see Figure 13) causing significant decrease in the alloy toughness.

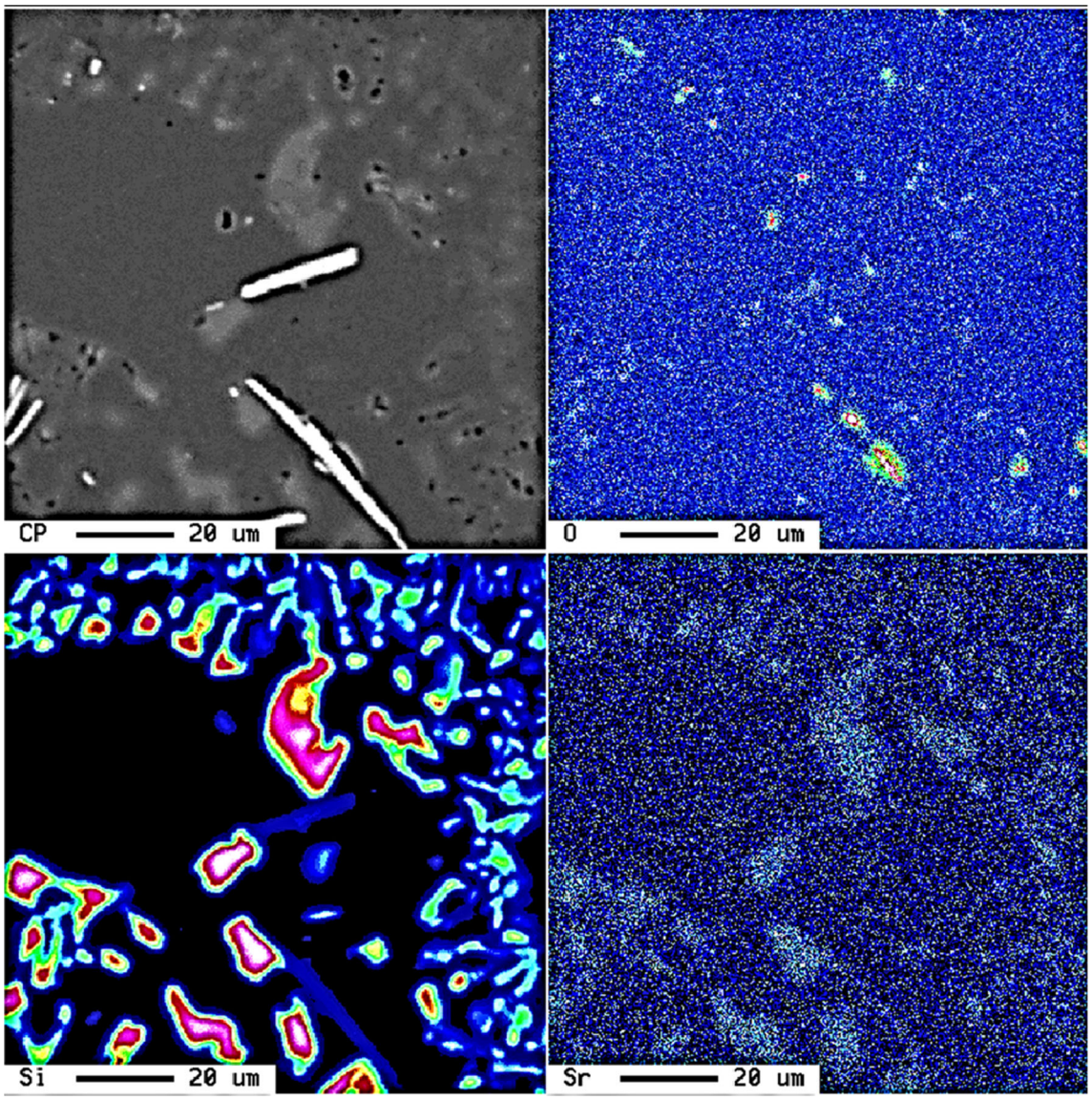

Figure 14. Effect of Sr addition on the morphology and size of both eutectic Si and Al_3Ti phase particles.

Table 5. Age-Hardening Behavior of A319 Alloy[30]

Stage	Heat treatment	Phases
I	None	Mostly precipitated as equilibrium $CuAl_2$ phases
II	Solution treatment and rapid cooling	All Cu in solution
		Most Mg phases in solution
III	Natural aging at room temperature	Segregation into GP I zones (coherent)
IV	Age hardening at 180 °C	Dissolution of GP I zones
		Segregation into GP II zones (coherent)
		Precipitation of S' phase ($CuAl_2Mg$)
	Further age hardening at 180 °C	Increased diffusion into GP II zones and precipitation as θ phase (partially coherent)
		Precipitation of S' phase ($CuAl_2Mg$)
		Precipitation of β' phase
		Precipitation of traces of Si
V	Overaging resulting from treatment time too long	Precipitated as θ phase, the equilibrium phase (incoherent)

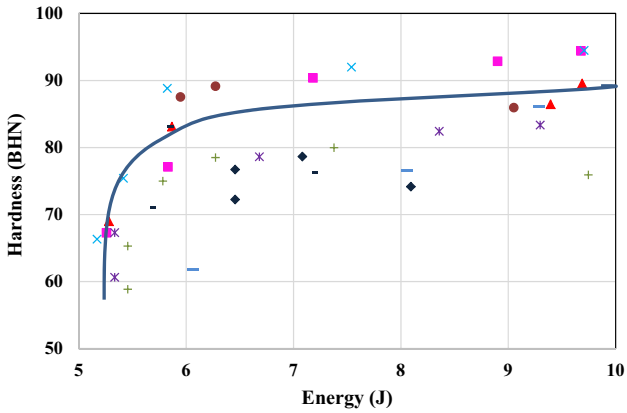

Figure 15. Hardness–total energy (E_t) relationship as a function of the applied melt treatment and aging temperature- same legend as in Figure 11.

3. Addition of Sr to high Ti-containing alloys negates the negative effect described above through both modification of the eutectic Si and fragmentation of the Al_3Ti platelets as shown in Figure 14.
4. Presence of oxide films (no degassing, Figure 10a) or severe porosity (Figure 10b) results in poor toughness (max 8 J).
5. All curves reveal multiple peaks, one at 180 °C and the other at 240 °C.

Andrade-Gonzalez et al.[30] reported a similar observations in grain refined, Sr-modified A319 alloy (alloy ADMS in the present case) during the aging process. According to the authors, the structural changes during the age-hardening process, in reality, are not so easy to distinguish. With increasing aging temperatures, different decomposition and precipitation processes take place in sequence, in some cases, and simultaneously in others. This can be shown in detail by considering the A319 alloy of this study. In this alloy, five stages of structural changes can be determined during the heat-treating operations. These are summarized in Table 5.

Hardness–total energy (E_t) relationships for all conditions investigated in the present study are presented in Figure 15. As can be seen, the hardness increased initially from 60BHN to 80BHN within less than 1 J followed by more or less a plateau up to 5 J with marginal increase in the alloy hardness. Thus, it is evident that the hardness is less sensitive to melt treatment compared to impact toughness.

Figure 16 represents vertical sections beneath the fracture surface of the ADT alloy sample. Due to the presence of long acicular Si particles, the fracture path (thin arrow) takes place through the non-modified particles (thick arrows). Although solution heat treatment improved the morphology of the Si particles—as highlighted in the black-circled area in Figure 16b, these particles could still contribute to crack propagation across the fracture surface (open arrows). Due to the fact that the Si particles are surrounded by the elastic aluminum matrix, cracking is confined to the Si particles (black arrows).

The retention of undissolved Cu-based intermetallic phase (possibly a mixture of Al_2Cu and Al_7Cu_2Fe phases) shown in Figure 16c also facilitates the crack propagation. The inset micrograph in Figure 16c reveals the presence of ultra-fine Si particles within the Cu phase indicating the end of solidification.[31] Modification of the ADT alloy with Sr (i.e., ADTS alloy) significantly improved the resistance to crack propagation as inferred from Figure 17a. The white arrows in this figure point to fine spherical Si particles that are enveloped by the aluminum matrix. Comparing Figures 16a and 17a clearly shows the change in the shape of the dendrites (see black arrows in Figure 17a).

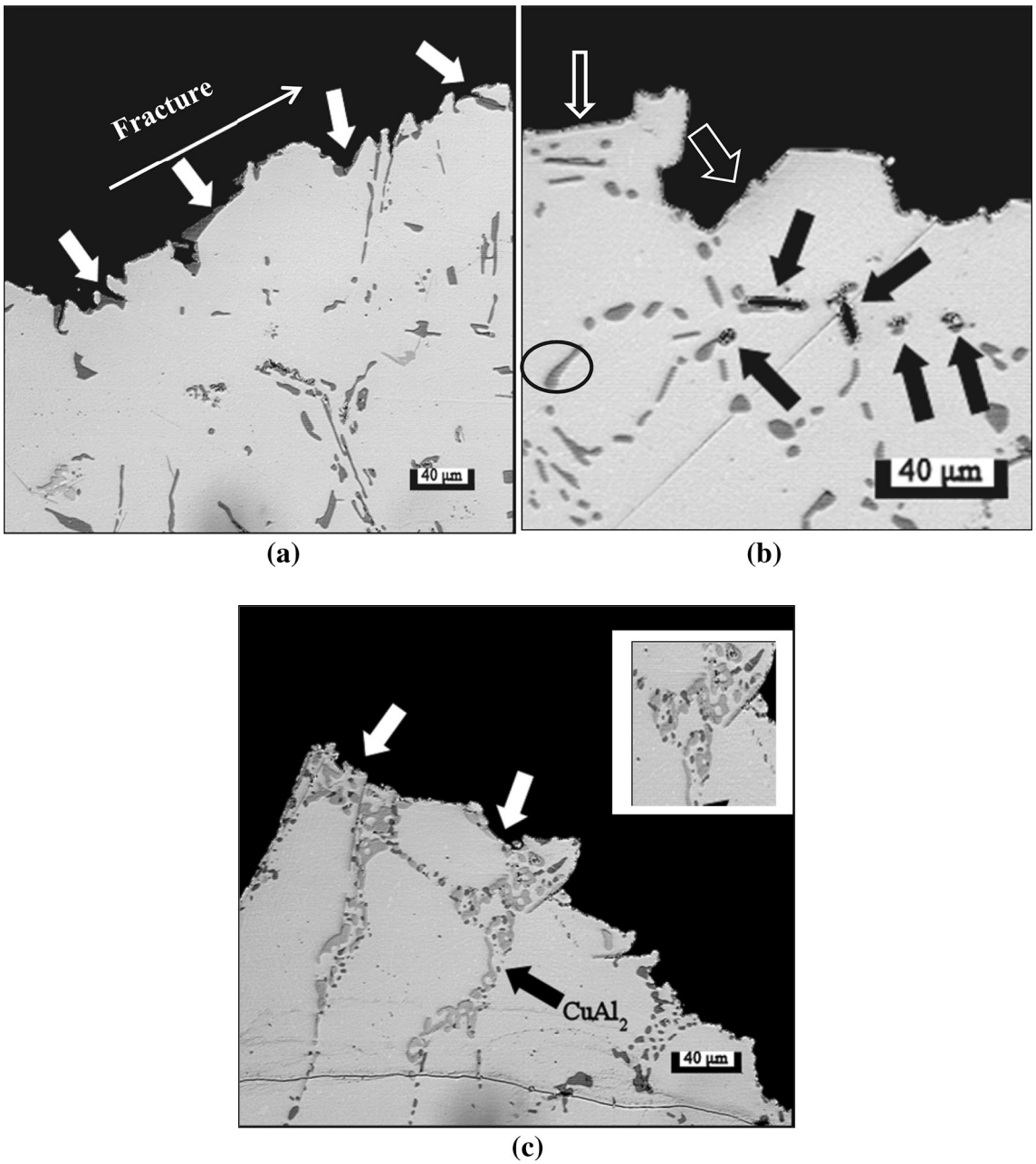

Figure 16. Sections beneath the fracture surface of ADT alloy: (a) in the as-cast condition, (b) after solutionizing treatment, (c) a relatively low magnification image of (b). Thin arrow in (a) shows the fracture path.

Following the solution heat treatment and associated increase in the alloy ductility,[10] the dendrites are more rounded with pin-point tips—black arrows.[32]

Conclusions

Based on the results documented in the present article, the following conclusions may be drawn:

1 The A319 aluminum alloy exhibiting the optimum combination of impact properties corresponds to the Sr-modified alloy with addition of Mg.

2 The Sr-modification process does not affect the aging behavior of the alloy while the addition of Mg enhances its response to artificial aging.

3 The strengthening effect observed in the alloy is due mainly to the presence of θ-Al_2Cu particles which precipitate in the form of needles and plates. The degree of strengthening that may be obtained depends directly on the amount and homogeneity of the θ-Al_2Cu phase.

4 The alloy does not exhibit the common peak-overaging characteristics normally reported in the literature. This observation may be attributed

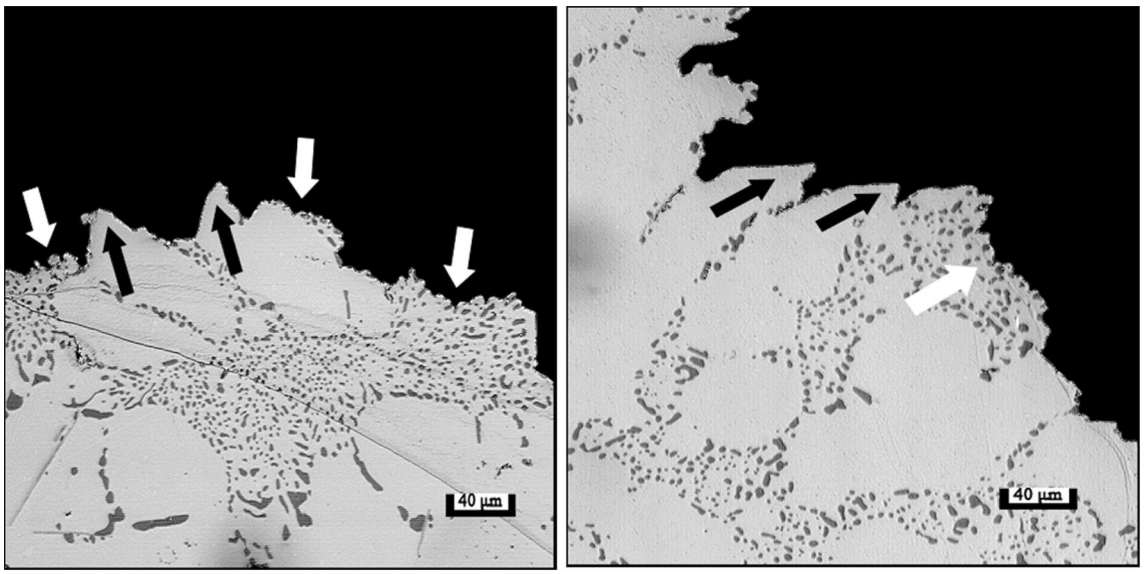

Figure 17. Sections beneath the fracture surface of the ADTS alloy sample: (a) in the as-cast condition, (b) after solutionizing treatment.

to the presence of sequential precipitation of different species during the aging process.

5 Hardness is less sensitive to melt treatment conditions.

6 Modification with Sr improves the alloy resistance to fracture during impact testing due to the larger volume fraction of the ductile aluminum matrix compared to non-modified alloys.

7 Increasing the amount of added grain refiner in terms of Ti content, i.e., 0.25 %Ti leads to the precipitation of large platelets of Al_3Ti phase and hence low impact energy.

8 Addition of Sr to high Ti-containing alloys negates the negative effect of Al_3Ti platelets through the change in the morphology and size of both eutectic Si particles and the Al_3Ti platelets.

9 Highest alloy toughness is obtained when the alloy is degassed, Sr modified and grain refined with optimum Ti content ($\sim$0.15 %Ti).

10 Porosity up to 2.6 vol% has a major influence on the alloy toughness.

Acknowledgments

The authors would like to thank Amal Samuel for enhancing the quality of the art work in the present article.

REFERENCES

1. Z. Li, A.M. Samuel, F.H. Samuel, C. Ravindran, S. Valtierra, H.W. Doty, Parameters controlling the performance of AA319-type alloys, Part I. Tensile properties. Mater. Sci. Eng. A **A367**, 96–110 (2004)
2. Z. Li, A.M. Samuel, F.H. Samuel, C. Ravindran, S. Valtierra, H.W. Doty, Parameters controlling the performance of AA319-type alloys, Part II. Impact properties and fractography. Mater. Sci. Eng. A **A367**, 111–122 (2004)
3. R.N. Lumley, I.J. Polmear, A.J. Morton, Development of mechanical properties during secondary aging in aluminum alloys. Mater. Sci. Technol. **21**, 1025–1033 (2005)
4. R.N. Lumley, I.J. Polmear, A.J. Morton, Development of properties during secondary ageing of aluminum alloys. Mater. Sci. Forum **426–432**, 303–308 (2003)
5. R.N. Lumley, I.J. Polmear, A.J. Morton, Interrupted aging and secondary precipitation in aluminum alloys. Mater. Sci. Technol. **19**, 1483–1491 (2003)
6. R.N. Lumley, A.J. Morton, G. O'Donnell, I.J. Polmear, New aluminum alloy heat treatment improves properties, reduces process costs. Ind. Heat. **71**, 31–34 (2004)
7. R.N. Lumley, I.J. Polmear, A.J. Morton, Control of secondary precipitation to improve the performance of aluminum alloys. Mater. Sci. Forum **396–402**, 893–898 (2002)
8. R.N. Lumley, I.J. Polmear, A.J. Morton, Novel ageing treatments to enhance mechanical properties of aluminum alloys, in: *J.T. Staley Honorary Symposium on Aluminum Alloys 'Materials Solutions 2001'*, Indiana, IN, ASM International, Materials Park, OH, pp. 248–254 (2001)
9. R.N. Lumley, I.J. Polmear, A.J. Morton, The utilisation of secondary ageing to improve the mechanical properties of aluminum alloys, in: *1st*

International Light Metals Technology Conference 2003, Brisbane, Australia, pp. 377–382 (2003)
10. P. Ouellet, F.H. Samuel, Effect of Mg on the ageing behaviour of Al–Si–Cu A319 type aluminum casting alloys. J. Mater. Sci. **34**, 4671–4697 (1999)
11. A.M. Samuel, H.W. Doty, S. Valtierra, F.H. Samuel, Effect of Mg addition of microstructure of A319 type alloys. Int. J. Cast Met. Res. **26**(6), 354–363 (2013)
12. M.M. Tash, F.H. Samuel, S.A. Alkahtani, Machinability of heat-treated 356 and A319 aluminum alloys: methodology for data processing and calculation of drilling force and moment. Adv. Mater. Res. **396–398**, 1008–1022 (2012)
13. Y. Han, A.M. Samuel, F.H. Samuel, H.W. Doty, J. Talamantes-Silva, S. American Foundry, parameters controlling the tensile properties of non-modified and Sr-modified Al–Si–Cu–Mg A319-type alloys, in *Metalcasting Congress*, vol. 117, American Foundry Society Las Vegas, Nevada (2009), pp. 169–186
14. F.J. Tavitas-Medrano, S. Valtierra, J.E. Gruzleski, F.H. Samuel, H.W. Doty, TEM study of the aging behavior of A319 type alloys, in *Metalcasting Congress*, vol. 112, American Foundry Society Atlanta, Georgia (2008), pp. 99–114
15. C.H. Caceres, M.B. Djurdjevic, T.J. Stockwell, J.H. Sokolowski, The effect of Cu content on the level of microporosity in Al–Si–Cu–Mg casting alloys. Scr. Mater. **40**, 631–637 (1999)
16. Z. Li, A.M. Samuel, F.H. Samuel, C. Ravindran, S. Valtierra, H.W. Doty, Factors affecting dissolution of CuAl2 phase in A319 alloys. AFS Trans. **111**, 241–254 (2003)
17. J. Gauthier, P.R. Louchez, F.H. Samuel, Heat treatment of A319.2 aluminum automotive alloy, part 1: solution heat treatment. Cast Met. **8**, 91–106 (1995)
18. N. Crowell, S. Shivkumar, Solution treatment effects in Cast Al–Si–Cu alloys. AFS Trans. **103**, 721–726 (1995)
19. A.M. Samuel, F.H. Samuel, C. Villeneuve, H.W. Doty, S. Valtierra, Effect of trace elements on β-Al_5FeSi characteristics, porosity and tensile properties of Al–Si–Cu (A319) cast alloys. Int. J. Cast Met. Res. **14**, 97–120 (2001)
20. M. Warmuzek, *Aluminum-Silicon Casting Alloys Atlas of Microfractographs* (ASM International, Materials Park, OH, 2004), p. 124
21. J.F. Hernandez-Paz, Heat treatment and precipitation in A356 aluminum alloy, Ph.D. Thesis, McGill University, Montreal, QC, Canada (2003), p. 112
22. J.E. Hatch (ed.), *Aluminum: Properties and Physical Metallurgy* (American Society for Metals, Materials Park, OH, 1984), p. 424
23. I.J. Polmear, *Light Alloys: Metallurgy of the Light Metals* (Wiley, New York, 1995), p. 362
24. M.A. Moustafa, F.H. Samuel, H.W. Doty, S. Valtierra, Effect of Mg and Cu additions on the microstructural characteristics and tensile properties of Sr-modified Al-Si eutectic alloys. Int. J. Cast Met. Res. **34**, 235–253 (2002)
25. D. Apelian, G.K. Sigworth, Fundamental aspects of heat treatment of cast Al–Si–Mg alloys. AFS Trans. **97**, 727–742 (1989)
26. D.A. Porter, K.E. Easterling, Phase Transformations in Metals and Alloys, Van Nostrand Reinhold (UK) Co. Ltd., Molly Millars Lane, Wokingham, Berkshire, England (1981), p. 446
27. H.T. Wu, C. Wang, S.K. Kung, The influence of grain refiner master alloy addition on A-356 aluminum alloy. J. Chin. Foundrym. Assoc. **29**, 10–18 (1981)
28. G.K. Sigworth, M.M. Guzowski, Grain refining of hypoeutectic Al–Si alloys. AFS Trans. **93**, 907–912 (1985)
29. M.M. Makhlouf, S. Shankar, Y.W. Riddle, Mechanisms of formation and chemical modification of the morphology of the eutectic phases in hypoeutectic aluminum–silicon alloys. AFS Trans. **113**, 145–162 (2005)
30. N.R. Andrade-Gonzalez, J.E. Gruzleski, F.H. Samuel, S. Valtierra and H.W. Doty, Effect of Mg and Sr additions in A319-type aluminum casting alloys, in *Proceedings of the International Symposium on Light Metals*, August 21–24, 2005, Calgary, Alberta, Canada. 2005: Calgary, AL, Canada. pp. 205–218
31. L. Bäckerud, G. Chai, J. Tamminen, Solidification characteristics of aluminum alloys, vol. 2 foundry alloys, AFS/Skanaluminium, Des Plaines, IL, USA, p. 1190
32. Z. Ma, A.M. Samuel, H.W. Doty, S. Valtierra, F.H. Samuel, Effect of Fe content on the fracture behaviour of Al-Si-Cu cast alloys. Mater. Des. **57**, 366–373 (2014)